Journal of the Optical Society of America B

OPTICAL PHYSICS

Semi-guided Gaussian beams

MANFRED HAMMER[1,2,*] AND JENS FÖRSTNER[1,2]

[1]Theoretical Electrical Engineering, Paderborn University, Paderborn, Germany
[2]Institute for Photonic Quantum Systems (PhoQS), Paderborn University, Paderborn, Germany
*manfred.hammer@uni-paderborn.de

Received 27 May 2026; revised 2 July 2026; accepted 16 July 2026; posted 16 July 2026; published 11 August 2026

Several recent proposals in integrated photonics concern components that operate on so-called semi-guided waves. Given a dielectric multilayer slab structure, these are wave solutions that propagate along the slab with the functional dependence of ordinary harmonic plane waves, but with modal confinement in the direction perpendicular to the slab plane. While the in-plane unbounded waves are valid as a theoretical construct, practical devices will have to work with laterally confined optical fields. To that end we consider Gaussian superpositions of semi-guided waves, for a range of in-plane propagation angles, here named "semi-guided Gaussian beams." This paper collects a series of relations that characterize these wave bundles, with emphasis on their divergence. The expressions resemble standard results for optical Gaussian beams, with modifications originating from the 1-D guiding and 1-D bundling. Examples for a high-contrast silicon-on-insulator slab at a typical telecom wavelength are discussed.

https://doi.org/10.1364/JOSAB.606932

1. INTRODUCTION

Some of the earliest concepts [1–3] discussed in the field of integrated optics [4–7] concern dielectric multilayer thin-film structures, and the propagation of thin-film guided, in-plane unguided light. Figure 1(a) illustrates that conception, for its perhaps simplest realization as a thin transparent waveguide core layer, sandwiched between two media with lower refractive index. Given certain conditions, the structure can "vertically" confine the light to the region around the core, while in-plane the waves exhibit the properties of standard harmonic plane waves, or superpositions of those. In the recent past, we have introduced the term *semi-guided waves* for these fields [8–11], as a means to distinguish them from free-space optical waves and light-beams (no guiding), on the one hand, and from the guided modes of optical channel waveguides, with two-dimensional confinement, on the other hand.

Proposals for on-chip equivalents of classical optical components, like lenses [12,13], mirrors [14], prisms [15,16], but also for more complex lens-systems [17], exploit the effects that transitions between regions with different dielectric layering have on these waves. Mostly, when looked at from a direction perpendicular to the film plane ("from the top"), the interfaces involved appear either straight or merely slightly curved. Hence, accepting certain approximations, standard results for the reflection and refraction of plane waves at dielectric interfaces can form the basis for a description of the in-plane propagation by geometrical optics [1,3]. Those studies, however, largely concern devices and material systems with comparably small or moderate refractive index contrast, where issues related to radiative losses do not play a (too serious) role.

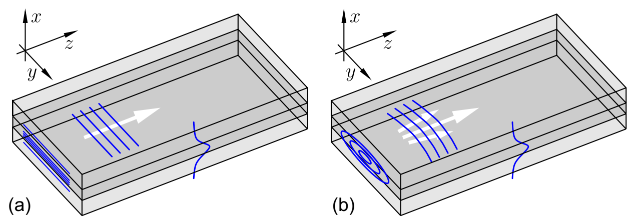

Fig. 1. Three-layer slab waveguide carrying a semi-guided wave (a), schematically. Bundles of these form a semi-guided beam (b). Cartesian coordinates are oriented such that x is perpendicular to the layer interfaces, while y and z span the slab plane.

More recent studies on devices that operate on the basis of semi-guided waves partly also cover traditional optical applications such as mirrors [18], power dividers and polarization beam splitters [19], diffraction gratings [20,21], lenses [22], or composite systems like entire spectrometers [23,24]. Other novel and perhaps somewhat surprising concepts concern, e.g., the lossless light propagation across 90° corners and respective step-like folds in optical slab waveguides [10,25–28], or lossless and largely reflectionless transitions between slab waveguides of different thicknesses [8,29,30].

The oblique propagation of semi-guided waves across channel waveguides, of different cross-sectional shapes, and with either direct or evanescent interaction, has been investigated in a series of different contexts. Some emphasis is on the spectral properties of bound states in the continuum (BICs) [31], predicted for oblique excitation of rectangular dielectric ridges by plane semi-guided waves [32–34], and by bundles of those [35–39].

Further, a variety of other optical filter functions can be realized. The examples include narrowband filters [40] based on a two-groove/ridge shape, high-Q resonances [41], and respective add-drop filter functions [42] realized by evanescent coupling of semi-guided waves to one or more rectangular dielectric strips, resonant absorbers [43], and filters constructed with coupled resonant ridges [44,45], also with emphasis on specific dispersion properties [46], on resonances of Fano-type [47], or on exploiting the particular features of "Diabolical points" [48]. Likewise, high-contrast waveguide Bragg gratings [49], operated with semi-guided waves at oblique angles, could be counted among those examples. Evanescent coupling of oblique semi-guided waves with channel waveguides with circular cross sections, i.e., with thin dielectric rods or tubes, enables the efficient excitation of optical waves that carry orbital angular momentum (OAM-waves) [50–52]. Wide ribs of specific dimensions, excited by semi-guided waves at normal angle, can act as simple interferometers, which have been investigated for application as polarizers [53] or optical isolators [54], and later for integrated optical (bio-) sensing [55,56].

The previous paragraphs concern optical components that work with the modes of mostly three-layer slab waveguides. Alternatively, also devices for semi-guided Bloch surface waves have been proposed. Among these are grooves that function as reflectors and beam splitters [57], as inversely designed focusing elements [58], or as integrated diffraction gratings [59,60].

Several of the former device concepts essentially require a high refractive index contrast, as shown by the discussion of critical angles for the suppression of radiative losses [10,11,25]. For our examples in Section 2.A, we therefore adopt parameters from the area of CMOS-compatible silicon photonics [61]. In that field, optical waveguides are mostly realized as so-called "photonic wires" [62]: these are single-mode channels with rectangular cross sections of sub-micrometer extension that provide extreme confinement of light waves, when, e.g., compared to typical optical fibers.

By contrast, the concepts for semi-guided waves exploit the respective material systems and associated layer stacks for quite different types of optical waves, with strong vertical, but often with no lateral confinement. Nevertheless, given some limited chip area, any attempts at realization of the proposals need to work with also laterally confined light. In line with the perhaps most prominent type of representation of laser beams [63–65], Gaussian bundles of semi-guided waves can be constructed by superimposing semi-guided waves for a range of lateral wavenumbers, or a range of propagation angles, respectively [10,51]. This leads to solutions of the Maxwell equations for the slab waveguide system as illustrated schematically in Fig. 1(b), here termed *semi-guided Gaussian beams*.

In several of the former studies, respective wave bundles serve for purposes of constructing laterally limited incoming fields for the components considered. While the angular spectrum of the bundles can well be relevant, the beam divergence usually does not play a role for the functioning of individual components. If one proceeds, however, toward a layout of composite chips that combine several components, all operating on semi-guided light, these beams will also serve for connecting components at larger on-chip distances. In this, the divergence of the laterally non-guided wave bundles will have to be considered.

Hence, in this paper, we carry the approximations one step further. Based on the rigorous expressions for Gaussian bundles of semi-guided waves in Section 2, and mostly following standard procedures for Gaussian beams, the integrals over lateral wavenumbers are evaluated including terms that cover the beam divergence. Section 3 then collects expressions that describe the characteristics of our semi-guided Gaussian beams.

2. GAUSSIAN BUNDLES OF SEMI-GUIDED WAVES

The guided slab modes [66,67] supported by the (multi-) layered dielectric structure under test form the basis for the semi-guided waves. Figure 1 introduces the relevant geometry. We adopt a formalism for electromagnetic fields $\boldsymbol{E}$, $\boldsymbol{H}$ in the frequency domain, with time dependence $\sim \exp(\mathrm{i}\omega t)$ for angular frequency $\omega = k\mathrm{c} = 2\pi\mathrm{c}/\lambda$, vacuum wavenumber k, wavelength λ, speed of light c, and vacuum permittivity ϵ_0 and permeability μ_0. For transparent and isotropic media, the waves satisfy the Maxwell equations in the frequency domain

$$\nabla \times \boldsymbol{E} = -\mathrm{i}\omega\mu_0 \boldsymbol{H}, \quad \nabla \times \boldsymbol{H} = \mathrm{i}\omega\epsilon\epsilon_0 \boldsymbol{E}, \tag{1}$$

where the slab structure is defined through the (often piecewise constant) relative permittivity $\epsilon = n^2$ or refractive index n, here both functions of the vertical coordinate x only.

Deviating somewhat from standard descriptions, we then consider solutions of Eq. (1) in the modal form

$$\begin{pmatrix} \boldsymbol{E} \\ \boldsymbol{H} \end{pmatrix}(x, y, z) = \Psi(x)\, \mathrm{e}^{-\mathrm{i}(k_z z + k_y y)}. \tag{2}$$

Each mode is characterized by an effective index N and a vectorial electromagnetic mode profile Ψ, with in-plane wavenumbers k_y and k_z that are related as $k^2 N^2 = k_y^2 + k_z^2$. These are the familiar "2-D" guided fields of TE and TM type [66,67], here rotated such that they propagate in the y-z plane at an angle θ with respect to the z axis, where $k_y = kN\sin\theta$. Detailed expressions for the rotated fields can be found, e.g., in Ref. [9]; respective solvers are readily available [68,69]. Note that the rotation concerns not only the direction of propagation, but also the lateral and longitudinal, electrical, and magnetic in-plane (y-, z-) components of the mode profiles. We would like to emphasize that the following discussion applies to arbitrary guiding multilayer stacks, or gradient-index waveguides, with a refractive index profile that depends only on x, and to guided (normalizability) slab modes of any polarization and order. Given a waveguide of interest, and having selected one specific guided mode supported by that slab, we then assume that the corresponding fields (2), for a range of angles θ, are at hand, computable through standard theory and algorithms.

We proceed with the bundling of these waves. As to be anticipated from the definition of θ, it is assumed that the constituting waves, and thus eventually the total beam, propagate in such directions in the y-z plane that a Fourier representation with integrals along k_y, or y, respectively, is adequate. This excludes beams that propagate in, or near to, the $\pm y$ direction; the formalism as discussed below could be applied, but a rotation of coordinates would be required. We focus on bundles with

Gaussian weight functions, and we restrict things to fields that build on one specific slab mode only.

Then, in line with the ansatz functions used in Refs. [10,51], the electromagnetic field ($\boldsymbol{E}$, $\boldsymbol{H}$) associated with a laterally limited semi-guided Gaussian beam can be constructed as follows:

$$\begin{pmatrix} \boldsymbol{E} \\ \boldsymbol{H} \end{pmatrix} (x, y, z) = A \int \mathrm{e}^{-\frac{(k_y - k_{y0})^2}{w_k^2}} \Psi(k_y; x) \times \mathrm{e}^{-\mathrm{i}[k_z(k_y)(z-z_0)+k_y(y-y_0)]} \mathrm{d}k_y. \tag{3}$$

Semi-guided waves (2) with a range of lateral wavenumbers k_y, or a range of propagation angles θ, are superimposed with a Gaussian weighting of half-width w_k. All waves correspond to one constituting slab mode with effective index N and profile Ψ; we here note explicitly the dependence (rotation) of the profile vector on the propagation angle or wavenumber k_y, respectively. For the purpose of Eq. (3), the longitudinal wavenumber

$$k_z(k_y) = \sqrt{k^2 N^2 - k_y^2} \tag{4}$$

becomes a function of k_y. The bundle propagates at primary angle θ_0, with a principal lateral wavenumber $k_{y0} = kN \sin\theta_0$. Coordinate offsets y_0 and z_0 determine the position of the beam focus.

The optical power carried by the bundle is given by integrating the z component of the time-averaged Poynting vector associated with the electromagnetic field (3) over the x-y plane, at some arbitrary, convenient z-position, e.g., at $z = z_0$. For a global amplitude

$$A = \left(w_k \sqrt{2\pi^3}\right)^{-1/2} \sqrt{l}, \tag{5}$$

the full beam is normalized to unit power, if, for all relevant k_y, the mode profiles $\Psi(k_y; x)$ are normalized to unit power per length unit l in direction y [9,53].

Assuming that Ψ and N represent the correct mode solutions for the dielectric stack in question, by construction any fields in the form of (3) solve the Maxwell equations exactly. The simulations of semi-guided beams in Refs. [10,19,29,49,51,52] rely on that representation, where Eq. (3) covers only the excitation part of those fields.

In case of slab waveguides made from isotropic media, and in case of homogeneous slabs without any obstacles, all directions in the y-z plane are equivalent. Correspondingly, we can then simplify things by selecting the z axis as the primary direction of propagation for the beam, with propagation angle $\theta_0 = 0$ and principal wavenumber $k_{y0} = 0$. Further, we place the focus at $(z_0, y_0) = (0, 0)$. This reduces Eq. (3) to

$$\begin{pmatrix} \boldsymbol{E} \\ \boldsymbol{H} \end{pmatrix} (x, y, z) = A \int \mathrm{e}^{-\frac{k_y^2}{w_k^2}} \Psi(k_y; x) \; \mathrm{e}^{-\mathrm{i}[k_z(k_y)z+k_y y]} \mathrm{d}k_y. \tag{6}$$

Besides the constituting slab mode, merely the spectral width w_k remains as a defining quantity. Equation (6) constitutes a bundle of exact continuous wave solutions of the Maxwell equations in the frequency domain, at fixed angular frequency ω, with a principal direction z of propagation, for varying in-plane transverse wavenumbers k_y. With respect to the direction x normal to the slab plane, the field remains guided, i.e., localized around the slab waveguide core, as enforced by the shape of the slab mode profile Ψ. What concerns the in-plane direction y, the bundle is localized in wavenumber space around the principal wavenumber $k_{y0} = 0$, with the spectral width w_k. The spatial localization along y shall become evident through the examples and theory in the following sections. Note that we here construct the beam in a bottom-up way, by superimposing analytic modal solutions. Up to this point, no approximations enter.

A. Examples

We adopt typical parameters for Si/SiO_2 waveguides at an optical telecommunication wavelength. A symmetric three-layer slab with a core of refractive index 3.45, with a thickness of 220 nm, is sandwiched between substrate/buffer and cladding layers with refractive index 1.45, for light at vacuum wavelength $\lambda = 1.55$ µm. The layer stack supports two guided modes [68], a fundamental TE mode with effective index $N = 2.8227$, and a fundamental TM mode with effective index $N = 2.0397$. Figures 2 and 3 illustrate the light propagation for polarized beams built from these modes, with different widths at focus. The recipes Eqs. (3) and (6) are applied, with rigorous numerical evaluation of the integrals through Gaussian quadrature. For the narrower bundles, the beam divergence becomes clearly apparent.

Differences between polarizations manifest mainly in the different mode profile shapes, which, in line with Eq. (6), transfer directly to the beams. For the present plots of absolute local electric field strength, the TM fields thus show the prominent discontinuities of the strong vertical electric x component of the TM mode, and a local minimum of $|\boldsymbol{E}|$ at the slab center $x = 0$ (both the normal and longitudinal electric profile components of the TM mode contribute). The color scales have been adjusted such that section plots for the same beam are comparable. Therefore, the "top-views," panels (a) and (e) of Fig. 3, evaluated at $x = 0$, show field levels that are lower than those at the core interfaces at $x = \pm 0.11$ µm (one-sided limits from outside the core layer). For the same width at focus, the TM beam exhibits, in terms of propagation distance z, a moderately "faster" divergence than the TE wave. According to the approximate analysis in the next section, this is related to the lower effective index N of the constituting TM slab mode.

3. BEAM CHARACTERISTICS

As shown, e.g., in Refs. [10,51], the integrals Eqs. (3) and (6) permit to include terms that cover the propagation across y-homogeneous obstacles of in principle arbitrary shape, and they are reasonably convenient for numerical evaluation. For easier assessment of the propagation characteristics of the bundle, however, some explicit expression, without the need for integration, would be useful. To that end, we introduce the following approximations:

- A small spectral width w_k is assumed, such that only *paraxial* waves with small deviations $|k_y - k_{y0}|$ in y-wavenumber

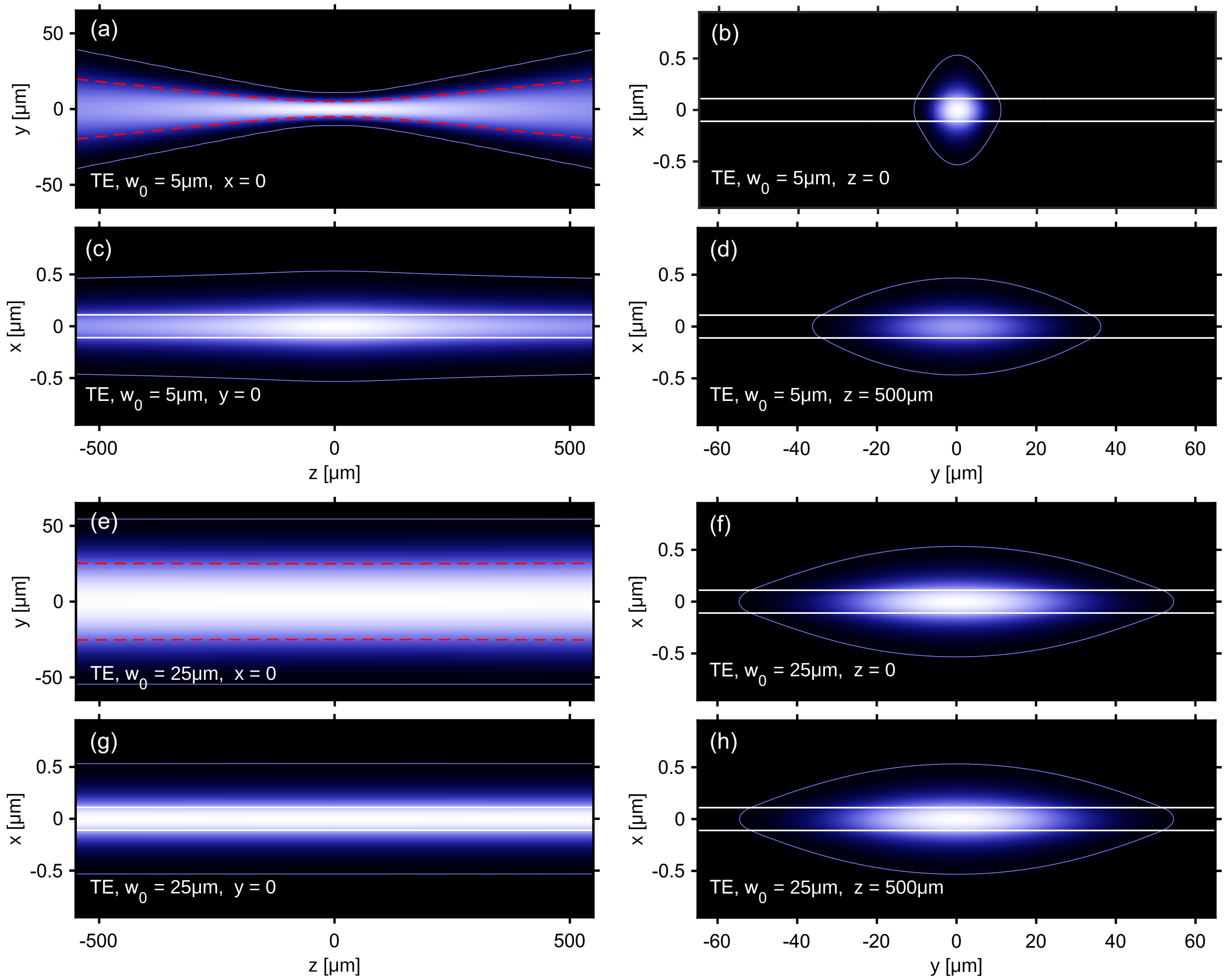

Fig. 2. TE-polarized semi-guided Gaussian beams of half-widths $w_0 = 5$ μm (a)–(d) and $w_0 = 25$ μm (e)–(h), propagation over a distance of 1 mm, focus at $z = 0$, rigorous numerical evaluation of Eqs. (3) and (6), with $w_k = 2/w_0$. Levels of the absolute electric field $|\boldsymbol{E}|$ are shown, on the horizontal plane at the slab center (a), (e), on the vertical plane along the beam axis (c), (g), and on cross-sectional planes at the focus (b), (f) and at a distance of 0.5 mm to the focus (d), (h). Colors are comparable among panels within the sets (a)–(d) and (e)–(h); contour lines (solid) are placed at the level of 1% of the maximum field strength. The in-plane shape of the beam can be captured well by the theory of Section 3: The dashed lines in (a), (e) indicate the 1/e-widths of the bundles according to Eq. (11).

[Eq. (3)], or with small absolute wavenumbers $|k_y|$ [Eq. (6)] contribute with significant weights to the integrals. One can then approximate, in Eqs. (3) and (6), the expression (4) for $k_z(k_y)$ by the first terms of its Taylor series expansion at $k_y = k_{y0}$.

- In principle, the mode profile Ψ depends on the lateral wavenumber k_y; the profile needs to be rotated according to the angles attributed to the individual waves. With a view to the small spectral width, we neglect that dependence and replace the profile by its vectorial value at the principal wavenumber k_{y0} [0 for Eq. (6)], as $\Psi(k_y, x) \approx \Psi(k_{y0}, x)$.

Subsequently, the analytical evaluation of the integrals becomes feasible.

In case of the bundle (3) with potentially oblique primary direction of propagation, these steps lead to the simpler expressions discussed in Refs. [10,51]. Only terms up to first order of the series expansion of $k_z(k_y)$ are included in the derivation. Being sufficient for the purposes of those papers, the resulting expressions characterize appropriately the spatial shape of the beams at their foci and the oblique propagation.

In order to capture also the beam divergence, we now restrict things to the simpler z-propagating bundle (6). The expansion of the longitudinal wavenumber is continued up to second order; the first-order term vanishes for the expansion at $k_y = 0$. Then k_z is approximated as

$$k_z(k_y) \approx kN\left(1 - \frac{k_y^2}{2k^2N^2}\right). \tag{7}$$

This results [63,64,70] in the following approximate expression for the z-axis aligned beam,

$$\begin{pmatrix} \boldsymbol{E} \\ \boldsymbol{H} \end{pmatrix}(x, y, z) = A\,\Psi(0; x)\,\frac{2\sqrt{\pi}}{\rho(z)}\;\mathrm{e}^{-\frac{y^2}{\rho^2(z)}}\;\mathrm{e}^{-\mathrm{i}kNz}, \tag{8}$$

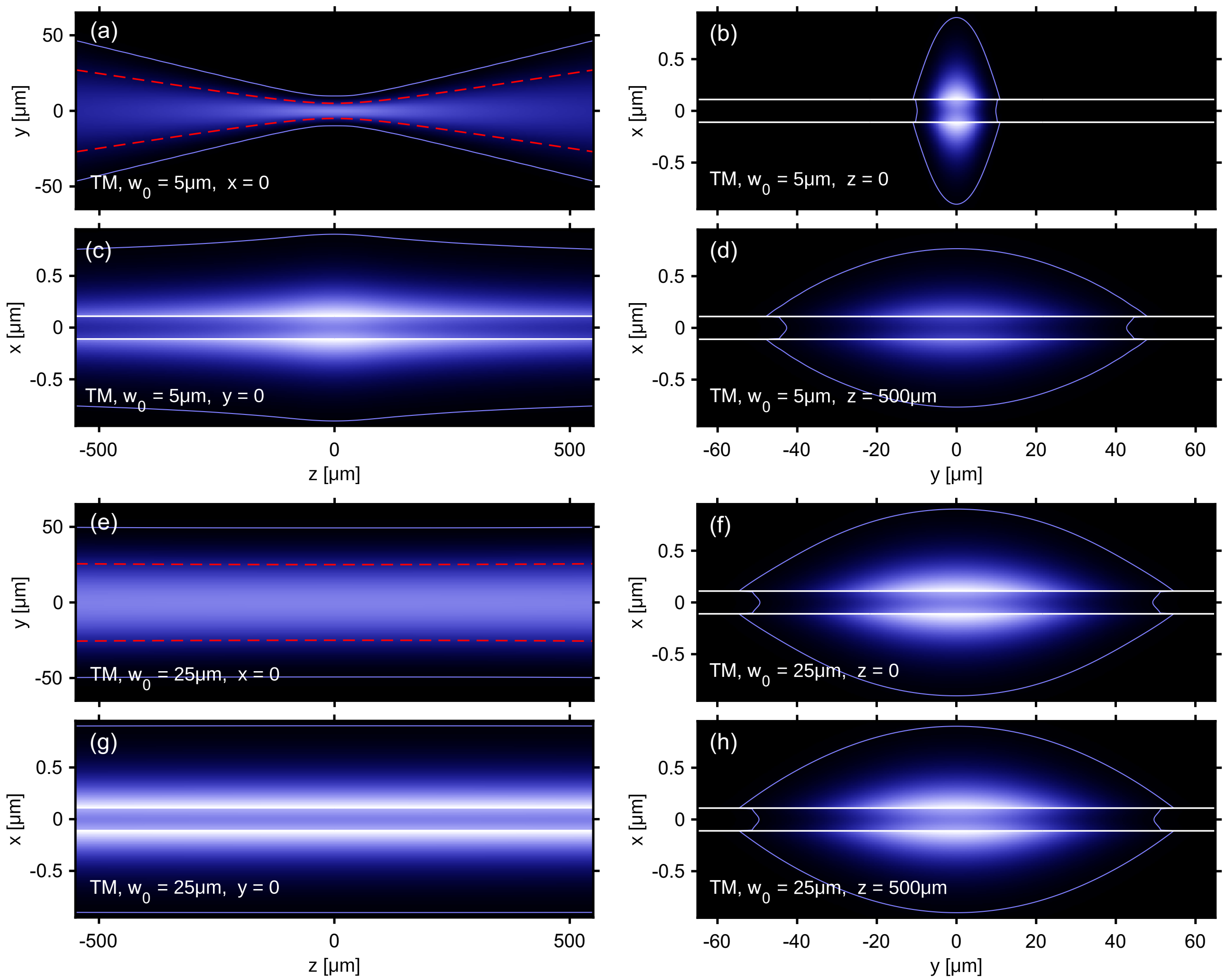

Fig. 3. TM-polarized semi-guided Gaussian beams of half-widths $w_0 = 5$ µm (a)–(d) and $w_0 = 25$ µm (e)–(h), propagation over a distance of 1 mm, focus at $z = 0$, rigorous numerical evaluation of Eqs. (3) and (6), with $w_k = 2/w_0$. Levels of the absolute electric field $|\boldsymbol{E}|$ are shown, on the horizontal plane at the slab center (a), (e), on the vertical plane along the beam axis (c), (g), and on cross-sectional planes at the focus (b), (f) and at a distance of 0.5 mm to the focus (d), (h). Colors are comparable among panels within the sets (a)–(d) and (e)–(h); contour lines (solid) are placed at the level of 1% of the maximum field strength. The analysis of Section 3 predicts the 1/e-widths of the bundles according to Eq. (11), indicated by the dashed lines in panels (a), (e).

with the shape and phase of the beam determined by the complex beam "radius"

$$\rho(z) = \frac{2}{w_k}\sqrt{1 - \mathrm{i}\frac{w_k^2 z}{2kN}}. \tag{9}$$

For a more convenient assessment, we write Eq. (8) in a form that is close to standard representations of (mostly free-space, 3-D) Gaussian beams, e.g., according to Refs. [63–65,71–73]. To that end the following quantities are introduced.

- The lateral spatial extension in-plane of the beam is characterized by the half-width

$$w_0 = \frac{2}{w_k} \tag{10}$$

in direction y at the focus position, the (half-) "waist" of the beam. This concerns the relative 1/e-level of the optical electromagnetic *field*.

- The bundle diverges longitudinally with a z-varying beam width

$$w(z) = w_0\sqrt{1 + \left(\frac{2z}{kNw_0^2}\right)^2} = w_0\sqrt{1 + \left(\frac{\lambda z}{\pi N w_0^2}\right)^2} = w_0\sqrt{1 + \frac{z^2}{z_R^2}}, \tag{11}$$

where $w_0 = w(0)$.

- At a longitudinal distance from the focus equal to the Rayleigh-length

$$z_R = \frac{1}{2}kNw_0^2 = \frac{\pi N w_0^2}{\lambda}, \tag{12}$$

the beam is wider by a factor of $\sqrt{2}$ when compared to the waist, $w(z_R) = \sqrt{2}\, w_0$.

- The shape of the wave fronts that constitute the beam is determined by the curvature radius

$$R(z) = z + \frac{z_R^2}{z} \tag{13}$$

at position z, the distance-to-source of a spherical wave with the same approximate parabolic local phase profile.

- The z-dependent Gouy phase φ_G, with

$$\tan[2\varphi_G(z)] = \frac{z}{z_R}, \tag{14}$$

specifies the deviation of the on-axis phase of the beam from the phase of a semi-guided plane wave, also related to mode Ψ, N, that travels in parallel to the bundle.

In these terms, and including Eq. (5) for the amplitude A, the power-normalized semi-guided Gaussian beam (8) can be given the form

$$\begin{pmatrix} \boldsymbol{E} \\ \boldsymbol{H} \end{pmatrix} (x, y, z) = \left(\frac{2}{\pi}\right)^{1/4} \sqrt{\frac{1}{w(z)}}\, \boldsymbol{\Psi}(0; x) \times \mathrm{e}^{-\frac{y^2}{w^2(z)}}\, \mathrm{e}^{-\mathrm{i}\frac{kNy^2}{2R(z)}}\, \mathrm{e}^{-\mathrm{i}[kNz-\varphi_G(z)]} \sqrt{l}. \tag{15}$$

The outcome is more or less identical to standard (approximate) expressions for Gaussian beams [63–65,71–73], with the exception of the presence of the slab mode profile Ψ and of the associated effective index N. Further, this concerns bundling only with respect to one transverse direction; hence, this corresponds to what one might consider as a 2-D Gaussian beam [71,73]. Differences to the 3-D expressions are found in the factor 2 in Eq. (14) for the Gouy phase and in the slower axial depletion $\sim 1/\sqrt{w(z)}$. As before, we assume that the profile Ψ is normalized to unit power per length unit l.

All former expressions rely on the restriction (7) of the series expansion of the longitudinal wavenumber (4), seen as a function of k_y, or of $k_y/(kN)$, respectively. For the approximation to be valid, only transverse wavenumbers k_y with $|k_y/(kN)| \ll 1$ should contribute with substantial weights to the bundle (6). This holds for a spectral width w_k that is small, $w_k/(kN) \ll 1$, when compared to the original propagation constant kN of the constituting slab mode. According to Eq. (10), we can thus expect the approximation to be adequate for beams with a half-width at focus w_0 that is large, $\pi N w_0/\lambda \gg 1$, when compared to the in-plane wavelength λ/N of the underlying semi-guided waves.

A. Beam Divergence

The in-plane divergence of the semi-guided beam is primarily characterized by the longitudinally varying width (11). Figure 4(a) shows a few respective curves, for the parameters as introduced for Figs. 2 and 3. The polarization enters through the modal effective index N, leading to pronouncedly different Rayleigh lengths (12), cf. Fig. 4(b), and to different divergence rates, for TE- and TM-polarized beams with the same (narrow) widths at focus.

Far away from the focus, the curves $[z, \pm w(z)]$ that border the beam at the $1/e$ field level tend to straight lines. These enclose an angle $\alpha_{1/2}$ with the beam axis, given by $\tan\alpha_{1/2} = w(z)/|z|$. In a limit of large distance $|z| \gg z_R$, when compared to the Rayleigh length z_R, this in-plane beam angle can be approximated as

$$\alpha_{1/2} \approx \frac{w_0}{z_R} = \frac{2}{kNw_0} = \frac{\lambda}{\pi N w_0}. \tag{16}$$

Note that $\alpha_{1/2}$ denotes only half of the full in-plane opening angle ("cone") of the semi-guided beam. Differences between TE- and TM-polarized bundles can be observed also in this quantity, as shown in Fig. 4(c).

"Diffraction" here evidently concerns the 2-D, in-plane propagation with respect to coordinates y and z only. According to, e.g., Eq. (12) for the Rayleigh length, or Eq. (16) for the beam angle, the beam divergence is governed by the effective index N of the constituting slab mode, rather than (directly) by the actual properties of the media that make up the slab waveguide. Beam diffraction depends, through N, on all parameters that influence the guidance properties of the slab [66–68], i.e., on its refractive index profile, on polarization and vacuum wavelength, and on the order of the selected mode. Potential effective indices N are limited to the range $\max_{x=\pm\infty}(n) < N < \max_x(n)$, where $n(x)$ is the refractive index profile of the slab. Given a mode, the semi-guided beams then diffract in-plane adhering to the rules for 2-D Gaussian beam propagation in a homogeneous (effective) medium with index N.

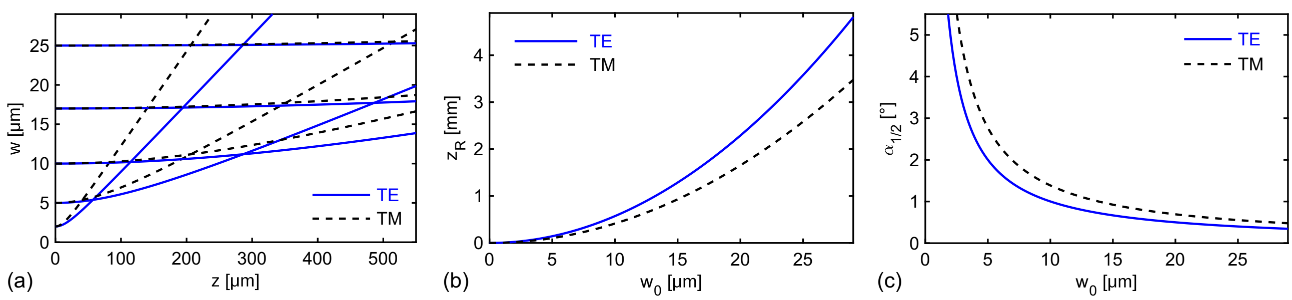

Fig. 4. Local half-width w versus distance-to-focus z of semi-guided Gaussian beams (a), for different values of the half-width at focus $w_0 \in \{2, 5, 10, 17, 25\}$ μm, and Rayleigh-length z_R (b) and in-plane opening angles $\alpha_{1/2}$ (c) as functions of w_0. This concerns bundles constructed from the fundamental TE- (continuous lines) and TM-modes (dashed lines) with effective indices $N_{TE} = 2.823$ and $N_{TM} = 2.040$, respectively [68], supported by a layer stack with refractive indices 1.45:3.45:1.45 with a core thickness of 220 nm, for vacuum wavelength $\lambda = 1.55$ μm.

B. Superpositions of Beams

Obviously, as long as one restricts to the linear regime, beams in the form of Eq. (3) can be superimposed to form further solutions of the Maxwell equations. For co-aligned beams constructed from different slab modes, the axial wavenumbers as well as Rayleigh lengths depend on modal effective indices, which, in general, differ between modes. Hence, even if through some excitation scheme the same width and a specific relative phase at focus could be effected, the partial beams diverge in phase and differ in width at other positions.

One might specifically consider a superposition of two z-propagating bundles (6), constructed of fundamental TE and TM modes. For evaluating the orientation of the electric field vector of that field, one has to take into account that the profiles of TM modes, but also the rotated profiles of TE modes, contain nonzero longitudinal components. In principle, the vectorial contributions of slab modes associated with directional beam components in Eq. (6) change with their angular orientation, i.e., with k_y. Further, the individual slab modes differ in shape, and therefore also their relative local contribution to the overall electric field of the beam varies along x. Hence, just as in other waveguide contexts, a discussion of "polarization" of the present beams should concern contributions of individual TE or TM modes, not the direction of some total transverse electric field vector.

In another respect, however, things are as simple as in free space optics: semi-guided beams as discussed here, irrespective of their constituting modes, can cross without any additional losses, reflections, or crosstalk, as one would have to expect for intersections of typical channel waveguides.

C. Further Effects

So far we restricted the discussion to some standard idealizations of optical waveguide theory: we looked at strictly guided modes supported by lossless isotropic, nonmagnetic dielectric slabs, given in terms of scalar real permittivity profiles. When stepping toward actual fabricated devices and their practical application, however, it might be necessary to consider further effects.

The present formalism relies on the Maxwell equations in the frequency domain; material dispersion can thus be captured by frequency-adapting the permittivity profiles of the slab, with consecutive slab mode analysis and bundling. The formation of pulsed semi-guided Gaussian beams, through frequency integration of Eq. (3) or (6), should thus be straightforward, in principle.

Then there are losses, either due to surface roughness [74,75], due to material attenuation [76], or caused by optical leakage [70], e.g., through the presence of a high contrast substrate below a buffer layer of insufficient thickness. Losses will also be present for all partly metallic slab structures that support surface-plasmon-polariton waves [77]. Slab waveguides with cores made of anisotropic media have attracted interest for already a long time, e.g., due to pronounced electrooptic or nonlinear properties of the materials [78] or as artificially constructed anisotropic metamaterials [79] with other (exotic) properties.

As long as one restricts things to the linear regime and provided that actual solutions to the slab mode problem are available, obtained either quasi-analytically [80,81] or by numerical means [79], assembly of semi-guided wave bundles along the recipe (3) should be possible. By construction, the beams then constitute exact solutions of the Maxwell equations, just as in the present idealized case. Any further approximate analysis, however, needs to be revised and potentially adapted.

As a rough first approach, one could assume that consequences of these additional effects on the slab mode properties, e.g., in the form of angular variations of mode profiles, or as potentially angle dependent real or imaginary shifts of slab mode effective indices, are small. One then proceeds with the bundling with modes that disregard these effects, applying the approximate theory and results for beam characterization as in Section 3. Finally, one computes an exact slab mode solution for the principal wavenumber k_{y0}, and attributes modal properties of that slab mode to the full beam, by adjusting N and Ψ in Eq. (15).

The bundling procedure as outlined in Section 2 requires the translational invariance of the slab profile in the two in-plane directions y and z. Thickness variations of the slabs can thus not be handled (directly). Structures of that category, however, give raise to certain phenomena as surveyed in Section 1, which caused the recent interest in semi-guided waves in the first place. These are thus well covered by other means of computational modeling.

4. CONCLUDING REMARKS

Based on largely analytical recipes for the construction of Gaussian bundles of semi-guided waves, we discuss approximate equations that govern their propagation. The beam divergence can be quantified through the Rayleigh length, or, alternatively, through the beam opening angle. These quantities are directly proportional/inversely proportional to the effective index of the constituting slab waveguide mode, such that high-contrast platforms like silicon-on-insulator appear advantageous for slower beam divergence. For the particular example of Fig. 4, a TE polarized beam of, e.g., 10 μm half-width at its central focus can bridge an on-chip distance of about 1 mm, while widening by merely 4 μm at its entry and exit positions.

One might thus envision the layout of an entire circuit, including several of the components for applications as listed in the introduction. In that process, the beam characteristics, specifically the divergence, but also the angular spectrum, have to be taken carefully into account. On the one hand, the beam divergence directly relates to the lateral width occupied by the light paths and thus to the space on-chip. Hence, if one considers longer distances between components, it might be necessary to include focusing elements, such as weak lenses [12,13,22] or slightly curved mirrors [14,24].

On the other hand, by construction, a narrower focus leads to a wider angular beam spectrum. The functioning of a component is often limited to some maximum angular range, i.e., requires incoming beams of some minimum width. This applies in particular to structures that rely on more or less sharp resonances of various kinds. The width can be substantial, as it is, e.g., for the spectral filters discussed in Ref. [49]. The former relations, and figures similar to Fig. 4, can then be instrumental for estimating the size of composite photonic circuits that operate on the basis of semi-guided waves and for their design in general.

Funding. Deutsche Forschungsgemeinschaft (231447078–TRR 142 (B06)); Ministerium für Kultur und Wissenschaft des Landes Nordrhein-Westfalen (PhoQC).

Disclosures. The authors have no competing interests to declare that are relevant to the content of this paper.

Data availability. Data underlying the results presented in this paper are not publicly available at this time but may be obtained from the authors upon reasonable request.

REFERENCES

1. R. Ulrich and R. J. Martin, "Geometrical optics in thin film light guides," Appl. Opt. **10**, 2077–2085 (1971).
2. P. K. Tien, S. Riva-Sanseverino, R. J. Martin, *et al.*, "Two-layered construction of integrated optical circuits and formation of thin-film prisms, lenses, and reflectors," Appl. Phys. Lett. **24**, 547–549 (1974).
3. P. K. Tien, "Integrated optics and new wave phenomena in optical waveguides," Rev. Mod. Phys. **49**, 361–420 (1977).
4. T. Tamir, *Integrated Optics* (Springer Verlag, 1979).
5. W. Karthe and R. Müller, *Integrierte Optik* (Akademische Verlagsgesellschaft Geest & Portig K.-G, 1991).
6. R. März, *Integrated Optics — Design and Modeling* (Artech House, 1994).
7. R. G. Hunsperger, *Integrated Optics: Theory and Technology*, 4th ed. (Springer Verlag, 1995).
8. F. Çivitci, M. Hammer, and H. J. W. M. Hoekstra, "Semi-guided plane wave reflection by thin-film transitions for angled incidence," Opt. Quantum Electron. **46**, 477–490 (2014).
9. M. Hammer, "Oblique incidence of semi-guided waves on rectangular slab waveguide discontinuities: a vectorial QUEP solver," Opt. Commun. **338**, 447–456 (2015).
10. M. Hammer, A. Hildebrandt, and J. Förstner, "Full resonant transmission of semi-guided planar waves through slab waveguide steps at oblique incidence," J. Lightwave Technol. **34**, 997–1005 (2016).
11. M. Hammer, L. Ebers, A. Hildebrandt, *et al.*, "Oblique semi-guided waves: 2-D integrated photonics with negative effective permittivity," in *IEEE 17th International Conference on Mathematical Methods in Electromagnetic Theory (MMET)* (2018), pp. 9–15.
12. G. C. Righini, V. Russo, S. Sottini, *et al.*, "Geodesic lenses for guided optical waves," Appl. Opt. **12**, 1477–1481 (1973).
13. F. Zernike, "Luneburg lens for optical waveguide use," Opt. Commun. **12**, 379–381 (1974).
14. S. Misawa, M. Aoki, S. Fujita, *et al.*, "Focusing waveguide mirror with a tapered edge," Appl. Opt. **33**, 3365–3370 (1994).
15. C.-C. Tseng, W.-T. Tsang, and S. Wang, "A thin-film prism as a beam separator for multimode guided waves in integrated optics," Opt. Commun. **13**, 342–346 (1975).
16. C. S. Tsai and P. Saunier, "Ultrafast guided-light beam deflection/switching and modulation using simulated electro-optic prism structures in $LiNbO_3$ waveguides," Appl. Phys. Lett. **27**, 248–250 (1975).
17. G. C. Righini and G. Molesini, "Design of optical-waveguide homogeneous refracting lenses," Appl. Opt. **27**, 4193–4199 (1988).
18. W. P. Tresna, A. W. S. Putra, and T. Maruyama, "Optical-loss measurement of a silicon-slab waveguide," Curr. Opt. Photonics **4**, 551–557 (2020).
19. M. Hammer, L. Ebers, and J. Förstner, "Configurable lossless broadband beam splitters for semi-guided waves in integrated silicon photonics," OSA Continuum **4**, 3081–3095 (2021).
20. S. S. M. Khaleghi, P. Karimi, and A. Khavasi, "On-chip second-order spatial derivative of an optical beam by a periodic ridge," Opt. Express **28**, 26481–26491 (2020).
21. H. Xu and Y. Shi, "Silicon-waveguide-integrated high-quality metagrating supporting bound state in the continuum," Laser Photonics Rev. **14**, 1900430 (2020).
22. L. Ebers, M. Hammer, and J. Förstner, "Light diffraction in slab waveguide lenses simulated with the stepwise angular spectrum method," Opt. Express **28**, 36361–36379 (2020).
23. F. Çivitci and H. J. W. M. Hoekstra, "Design of spectrometers and polarization splitters using adiabatically connected slab waveguides," in *16th European Conference on Integrated Optics (ECIO)*, Sitges/Barcelona, Spain, 2012, p. 151.
24. F. Çivitci, M. Hammer, and H. J. W. M. Hoekstra, "Planar prism spectrometer based on adiabatically connected waveguiding slabs," Opt. Commun. **365**, 29–37 (2016).
25. M. Hammer, A. Hildebrandt, and J. Förstner, "How planar optical waves can be made to climb dielectric steps," Opt. Lett. **40**, 3711–3714 (2015).
26. A. Hildebrandt, S. Alhaddad, M. Hammer, *et al.*, "Oblique incidence of semi-guided waves on step-like folds in planar dielectric slabs: lossless vertical interconnects in 3D integrated photonic circuits," Proc. SPIE **9750**, 97501B (2016).
27. L. Ebers, M. Hammer, and J. Förstner, "Spiral modes supported by circular dielectric tubes and tube segments," Opt. Quantum Electron. **49**, 176 (2017).
28. L. Ebers, M. Hammer, and J. Förstner, "Oblique incidence of semi-guided planar waves on slab waveguide steps: effects of rounded edges," Opt. Express **26**, 18621–18632 (2018).
29. M. Hammer, L. Ebers, and J. Förstner, "Oblique quasi-lossless excitation of a thin silicon slab waveguide: a guided-wave variant of an anti-reflection coating," J. Opt. Soc. Am. B **36**, 2395–2401 (2019).
30. M. Hammer, J. Förstner, and L. Ebers, "Optischer Übergang zwischen zwei optischen Schichtwellenleitern und Verfahren zum Übertragen von Licht," German Patent DE 10 2018 108 110 B3 (31 January 2019) [Deutsches Patent- und Markenamt (filed 05.04.2018, issued 31.01.2019)].
31. C. W. Hsu, B. Zhen, A. D. Stone, *et al.*, "Bound states in the continuum," Nat. Rev. Mater. **1**, 16048 (2016).
32. C.-L. Zou, J.-M. Cui, F.-W. Sun, *et al.*, "Guiding light through optical bound states in the continuum for ultrahigh-Q microresonators," Laser Photonics Rev. **9**, 114–119 (2014).
33. E. A. Bezus, D. A. Bykov, and L. L. Doskolovich, "Bound states in the continuum and high-Q resonances supported by a dielectric ridge on a slab waveguide," Photonics Res. **6**, 1084–1093 (2018).
34. D. A. Bykov, E. A. Bezus, and L. L. Doskolovich, "Bound states in the continuum and strong phase resonances in integrated Gires-Tournois interferometer," Nanophotonics **9**, 83–92 (2020).
35. E. A. Bezus, L. L. Doskolovich, D. A. Bykov, *et al.*, "Spatial integration and differentiation of optical beams in a slab waveguide by a dielectric ridge supporting high-Q resonances," Opt. Express **26**, 25156–25165 (2018).
36. T. G. Nguyen, G. Ren, S. Schoenhardt, *et al.*, "Ridge resonance in silicon photonics harnessing bound states in the continuum," Laser Photonics Rev. **13**, 1900035 (2019).
37. S. Schoenhardt, A. Boes, T. G. Nguyen, *et al.*, "Ridge resonators: impact of excitation beam and resonator losses," Opt. Express **29**, 27092–27103 (2021).
38. S. Schoenhardt, A. Boes, T. G. Nguyen, *et al.*, "Ridge waveguide couplers with leaky mode resonator-like wavelength responses," Opt. Express **31**, 626–634 (2023).
39. P. Tang, S. Schoenhardt, G. Ren, *et al.*, "Ridge resonators with compact guided mode coupling," Opt. Express **31**, 34189–34200 (2023).
40. L. L. Doskolovich, E. A. Bezus, and D. A. Bykov, "Two-groove narrowband transmission filter integrated into a slab waveguide," Photonics Res. **6**, 61–65 (2018).
41. M. Hammer, L. Ebers, and J. Förstner, "Oblique evanescent excitation of a dielectric strip: a model resonator with an open optical cavity of unlimited Q," Opt. Express **27**, 9313–9320 (2019).
42. L. Ebers, M. Hammer, M. B. Berkemeier, *et al.*, "Coupled microstrip-cavities under oblique incidence of semi-guided waves: a lossless integrated optical add-drop filter," OSA Continuum **2**, 3288–3298 (2019).
43. E. A. Bezus, D. A. Bykov, and L. L. Doskolovich, "Total absorption and coherent perfect absorption in metal–dielectric–metal resonators integrated into a slab waveguide," Opt. Lett. **47**, 4403–4406 (2022).

44. T. G. Nguyen, K. Yego, G. Ren, *et al.*, "Microwave engineering filter synthesis technique for coupled ridge resonator filters," Opt. Express **27**, 34370–34381 (2019).
45. L. L. Doskolovich, E. A. Bezus, and D. A. Bykov, "Integrated flat-top reflection filters operating near bound states in the continuum," Photonics Res. **7**, 1314–1322 (2019).
46. E. A. Bezus, D. A. Bykov, and L. L. Doskolovich, "Integrated Gires–Tournois interferometers based on evanescently coupled ridge resonators," Opt. Lett. **45**, 5065–5068 (2020).
47. J. Chen and P. Chu, "Phase-induced Fano antiresonance in a planar waveguide with two dielectric ridges," J. Opt. Soc. Am. B **36**, 3417–3427 (2019).
48. J. Chen, L. Tang, L. Wang, *et al.*, "Diabolical points in coupled ridge resonators," J. Opt. Soc. Am. B **40**, 293–300 (2023).
49. M. Hammer, H. Farheen, and J. Förstner, "How to suppress radiative losses in high-contrast integrated Bragg gratings," J. Opt. Soc. Am. B **40**, 862–873 (2023).
50. M. Hammer, L. Ebers, and J. Förstner, "Hybrid coupled mode modelling of the evanescent excitation of a dielectric tube by semi-guided waves at oblique angles," Opt. Quantum Electron. **52**, 472 (2020).
51. M. Hammer, L. Ebers, and J. Förstner, "Resonant evanescent excitation of guided waves with high-order optical angular momentum," J. Opt. Soc. Am. B **38**, 1717–1728 (2021).
52. M. Hammer, L. Ebers, and J. Förstner, "Resonant evanescent excitation of OAM modes in a high-contrast circular step-index fiber," Proc. SPIE **12017**, 120170F (2022).
53. M. Lohmeyer and R. Stoffer, "Integrated optical cross strip polarizer concept," Opt. Quantum Electron. **33**, 413–431 (2001).
54. M. Lohmeyer, L. Wilkens, O. Zhuromskyy, *et al.*, "Integrated magnetooptic cross strip isolator," Opt. Commun. **189**, 251–259 (2001).
55. K. E. Zinoviev, A. B. Gonzalez-Guerrero, C. Dominguez, *et al.*, "Integrated bimodal waveguide interferometric biosensor for label-free analysis," J. Lightwave Technol. **29**, 1926–1930 (2011).
56. L. Torrijos-Morán, B. D. Lisboa, M. Soler, *et al.*, "Integrated optical bimodal waveguide biosensors: principles and applications," Results Opt. **9**, 100285 (2022).
57. R. Wang, J. Chen, Y. Xiang, *et al.*, "Two-dimensional photonic devices based on Bloch surface waves with one-dimensional grooves," Phys. Rev. Appl. **10**, 024032 (2018).
58. Y. Augenstein, A. Vetter, B. V. Lahijani, *et al.*, "Inverse photonic design of functional elements that focus Bloch surface waves," Light Sci. Appl. **7**, 104 (2018).
59. E. A. Bezus, D. A. Bykov, and L. L. Doskolovich, "Integrated diffraction gratings on the Bloch surface wave platform supporting bound states in the continuum," Nanophotonics **10**, 4331–4340 (2021).
60. E. A. Bezus, D. A. Bykov, L. L. Doskolovich, *et al.*, "Integrated resonant diffraction gratings for Bloch surface waves," Opt. Mem. Neural Netw. **31**, S8–S13 (2022).
61. R. Soref, "The past, present, and future of silicon photonics," IEEE J. Sel. Top. Quantum Electron. **12**, 1678–1687 (2006).
62. W. Bogaerts, D. Taillaert, B. Luyssaert, *et al.*, "Basic structures for photonic integrated circuits in Silicon-on-insulator," Opt. Express **12**, 1583–1591 (2004).
63. N. Lindlein and G. Leuchs, "Wave optics," in *Springer Handbook of Lasers and Optics*, F. Träger, ed. (Springer, 2007), Part A, Chap. 3, pp. 87–156.
64. O. Svelto, *Principles of Lasers*, 5th ed. (Springer, 2010).
65. J. Alda, "Laser and Gaussian beam propagation and transformation," in *Encyclopedia of Optical and Photonic Engineering*, C. Hoffman and R. Driggers, eds., 2nd ed. (CRC Press, 2015), pp. 1193–1207.
66. C. Vassallo, *Optical Waveguide Concepts* (Elsevier, 1991).
67. K. Okamoto, *Fundamentals of Optical Waveguides* (Academic, 2000).
68. M. Hammer, "OMS — 1-D mode solver for dielectric multilayer slab waveguides," https://www.computational-photonics.eu/oms.html.
69. M. Hammer, "METRIC — Mode expansion tools for 2D rectangular integrated optical circuits," https://metric.computational-photonics.eu/.
70. J. Hu and C. R. Menyuk, "Understanding leaky modes: slab waveguide revisited," Adv. Opt. Photonics **1**, 58–106 (2009).
71. COMSOL, "COMSOL documentation - Ray optics module - Section *Gaussian beam theory*," COMSOL Multiphysics GmbH, https://doc.comsol.com.
72. H. Kogelnik and T. Li, "Laser beams and resonators," Appl. Opt. **5**, 1550–1567 (1966).
73. R. L. Nowack and S. M. Kainkaryam, "The Gouy phase anomaly for harmonic and time-domain paraxial Gaussian beams," Geophys. J. Int. **184**, 965–973 (2011).
74. F. P. Payne and J. P. R. Lacey, "A theoretical analysis of scattering loss from planar optical waveguides," Opt. Quantum Electron. **26**, 977–986 (1994).
75. J. P. R. Lacey and F. P. Payne, "Radiation loss from planar waveguides with random wall imperfections," IEE Proc. J - Optoelectron. **137**, 282–289 (1990).
76. M. Miyagi, A. Hongo, and S. Kawakami, "Transmission characteristics of dielectric-coated metallic waveguide for infrared transmission: slab waveguide model," IEEE J. Quantum Electron. **19**, 136–145 (1983).
77. K. L. Tsakmakidis, C. Hermann, A. Klaedtke, *et al.*, "Surface plasmon polaritons in generalized slab heterostructures with negative permittivity and permeability," Phys. Rev. B **73**, 085104 (2006).
78. M. Hammer, H. Farheen, and J. Förstner, "Guided modes of thin-film lithium niobate slabs," Opt. Continuum **3**, 2024–2043 (2024).
79. Z. Guo, J. Song, H. Jiang, *et al.*, "Miniaturized backward coupler realized by the circuit-based planar hyperbolic waveguide," Adv. Photonics Res. **2**, 2100035 (2021).
80. M. Hammer, "TFLNS — mode solver for three-layer thin film lithium niobate slab waveguides," https://www.computational-photonics.eu/tflns.html.
81. M. Hammer, "PlasS — 1-D mode solver for complex optical multilayer step-index slab waveguides," https://www.computational-photonics.eu/plass.html.